SUPERCONTINUUM GENERATION IN A SILICON NANOWIRE EMBEDDED PHOTONIC CRYSTAL FIBER FOR OPTICAL COHERENCE TOMOGRAPHY APPLICATIONS

E. Gunasundari[1], K. Senthilnathan[1], *P. Ramesh Babu[1], J. Ebenezar[2] and K.Nakkeeran[3]

[1]Department of Physics, School of Advanced Sciences, VIT University, Vellore-632 014, India.

[2]Department of Physics, Jamal Mohamed College (Autonomous), Tiruchirappalli-620 020, India.

[3]Department of Engineering, Fraser Noble Building, King's College, University of Aberdeen, Aberdeen AB24 3UE, U.K.

Abstract

In this paper, we design a silicon nanowire embedded photonic crystal fiber (SN-PCF) using fully vectorial finite element method. Further, we analyze the various optical properties, namely, waveguide dispersion and nonlinearity by varying the core diameter from 400 to 500 nm for a wide range of wavelengths from 0.8 to 1.7 μm. The proposed structure exhibits a low second (-0.4909 ps^2/m) and third order (0.6595 10^{-3}ps^3/m) dispersions with very high nonlinearity (1358 W^{-1}m^{-1}) for 480 nm core diameter at 0.8 μm wavelength. Besides, we investigate the evolution of supercontinuum at 0.8 μm, 1.3 μm and 1.55 μm wavelengths for an incredibly low input pulse energy of 2.5 pJ. The numerical results corroborate that the proposed SN-PCF provides a wider supercontinuum bandwidth of 1250 nm at 0.8 μm, 1100 nm at 1.3 μm and 800 nm at 1.55 μm wavelengths. We demonstrate longitudinal resolution of 0.16 μm at 0.8 μm wavelength for ophthalmology and dermatology, 0.41 μm at 1.3 μm wavelength for dental imaging and 0.8 μm at 1.55 μm wavelength also for dental imaging. To our knowledge, these are the highest resolution ever achieved in biological tissue at 0.8 μm, 1.3 μm and 1.55 μm wavelengths.

Keywords: Photonic crystal fiber, Silicon nanowire, Optical properties, Supercontinuum generation and Optical coherence tomography.

1 Introduction

Optical coherence tomography (OCT) is a new technology for noninvasive cross-sectional imaging of tissue structure in biological system by directing a focused beam of light at the tissue to be imaged (2). This technique is used for both transparent and non-transparent biological tissues and its performance depends on longitudinal (axial) and transverse (lateral) resolution, dynamic range, measurement speed and center wavelength of light source. Nowadays, OCT is used for not only opthalmology but also for dermatology, dental as well as for the early detection of cancer in digestive organs. Previously, typical sources for OCT applications were superluminescent

---

*prameshbabu@vit.ac.in

diodes (SLDs) and sources based on an amplified spontaneous emission (ASE) from doped fibers or semiconductors (3). All of these sources have a limited spectral bandwidth and a restricted wavelength range. Therefore, SLDs having 10 to 15 μm longitudinal resolutions that are used for most of the standard OCT applications are being replaced with PCF based supercontinuum (SC) light sources (3; 4).

The wavelength range of the OCT light source is spread from 0.8 to 1.6 μm wavelength. This wavelength region is of particular interest for OCT because it penetrates deeply into biological tissue and permits spectrally resolved imaging of water absorption bands, (5). In the spectral region, loss is minimum due to absorption and scattering. Ultrahigh-resolution OCT imaging in the spectral region from 0.8 to 1.6 μm requires extremely broad bandwidths because longitudinal resolution depends on the coherence length. The coherence length is inversely proportional to the spectral width and proportional to square of the center wavelength of the light source. This can be achieved by SC using PCFs. The opthalmology and dermatology OCT imaging are mainly operated at near 0.8 μm center wavelength (2; 6). The dentistry OCT imaging is done at 1.3 μm wavelength (7). Currently, the broadband light source can be employed to take the OCT image of human tooth samples at 1.5 to 1.6 μm, (8).

Recently, the research focus is on SC as it happens to be one of the proven techniques for the generation of high intense ultrafast broadband light source. It arises from the nonlinear interaction and propagation of ultrashort pulse in the nonlinear material. The SC light source is used in various fields such as ranging, imaging, remote sensing and computation. Most commonly used mcrostructured fibers to produce SC are photonic crystal fibers (PCFs), birefringent PCF, tapered fibers, hollow fibers, single and multiple sub-wavelength size core fibers and different material doped silica fibers (9)-(17). The PCFs turn out to be a very good platform to produce high power light source in OCT system. Because PCFs can produce wider SC spectrum due to their design flexibility which result in enhanced nonlinear effects by reducing the core area and by appropriately tailoring the dispersion characteristics. In a typical PCF based SC source, the effective mode area of the PCF is roughly ~ 1 μm^2 with several meter of PCF (18). Further, by reducing the core down to nm size and tapering the micro-structured core, the effective optical nonlinearity can be increased (19). Although these previous studies have demonstrated efficient generation of SC in on-chip integration, those sources demand a large propagation length for generating high spectral broadening.

A promising alternative solution is provided by silicon waveguide sources (20), which have the advantage of employing an emerging silicon-on-insulator (SOI) integrated-photonics platform. Silicon has excellent transmission properties compared to silica and does not require high power density to bring in nonlinearity owing to its huge nonlinear coefficient (21). Till date, many reports for SCG in silicon nanowire are available (19)-(22). Recently, the possibility of SCG of 500 nm bandwidth at telecommunication wavelength has been demonstrated with various input peak powers for various SOI waveguide lengths. Such a dielectric silicon waveguide with a nanocore diameter could provide a remarkably strong field confinement, enhanced light-matter interactions and strong tunable dispersions when embedded into PCF (23). The resulting silicon photonic device known as silicon nanowire embedded photonic crystal fiber (SN-PCF) has been proposed very recently (24). These small core structures are ideal devices for nonlinear processes such as pulse compression and SC generation within short fiber lengths (25)-(27).

In this work, we report a broadband SC in highly nonlinear SN-PCF at center wavelengths of 0.8 μm, 1.3 μm and 1.55 μm using low power (25 W) femtosecond pulses which can be used in ultrahigh-resolution OCT system for ophthalmology, dermatology and dental imaging. Section 2 presents the design analysis of the proposed structure through a full vector finite element method. In section 3, we explore the various optical properties including group velocity dispersion (GVD), third order dispersions (TOD), effective mode area and effective nonlinearity by varying the core diameter from 420 to 480 nm. We investigate the nonlinear pulse propagation in the anomalous
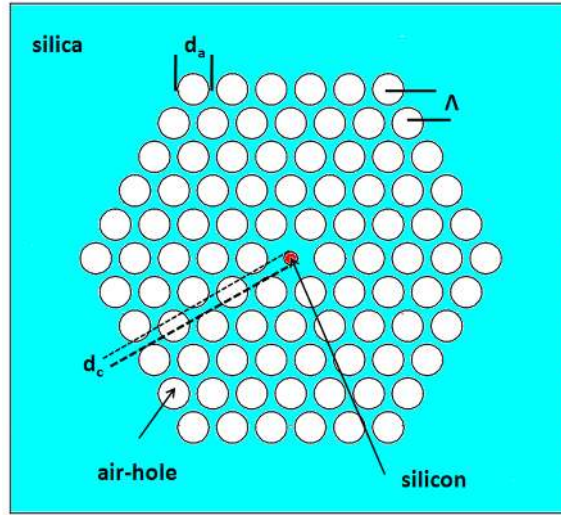
2

Figure 1: *Geometrical structure of the proposed SN-PCF with 480 nm core diameter*

dispersion regime and analyze the evolution of SC for 25 W input peak power of 2 mm length of SN-PCF for 480 nm core diameter in section 4. Finally, we summarize the findings in section 5.

2   Design of the proposed SN-PCF

The schematic cross section of the proposed SN-PCF is as shown in Fig. 1. It is composed of circular air holes in the cladding arranged in a triangular pattern and a circular nanosize core. Here, the air-hole diameter is 1120 nm and increasing the core diameter from 420 to 480 nm for analyzing the optical properties.

We have already explored all the optical properties for the various core diameters ranging from 1000 to 300 nm (24). In this work, we choose to vary the core diameter from 420 to 480 nm for analyzing the optical properties for a wavelength range from 0.8 to 1.7 μm for generating SC. The justification for this range of study is because of tight mode confinement within the core and nearly zero dispersion with high nonlinearity. Fig. 2 illustrates the mode field distribution at 0.8 μm wavelength for 480 nm core diameter. In order to determine the dispersion of SN-PCF, it is necessary to compute the effective refractive index of the fundamental mode and the same is done by finite element method. In Fig. 3, we plot the effective index as a function of wavelength for various core diameters.

3   Optical properties Of SN-PCF

In this section, we explore the various linear and nonlinear properties. In sub-section **??**, we study the impact of dispersions of fundamental mode for different core diameters. Finally, in sub-section **??**, we compute the effective nonlinearity by calculating the effective mode area.
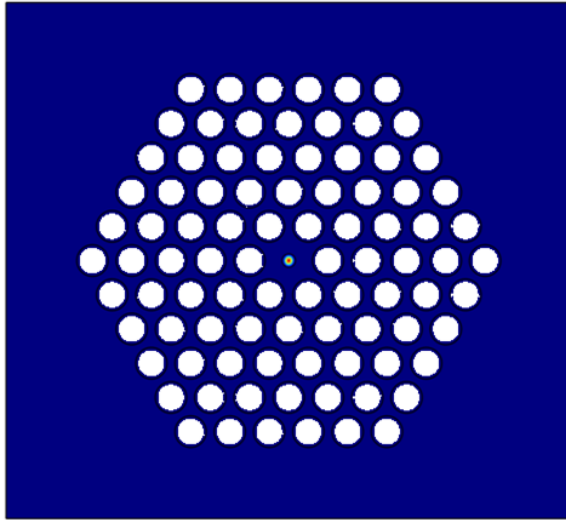
Figure 2: *Mode field distribution in (a) 2D view and (b) contour view of the proposed SN-PCF at 0.8 µm wavelength at 480 nm core diameter*
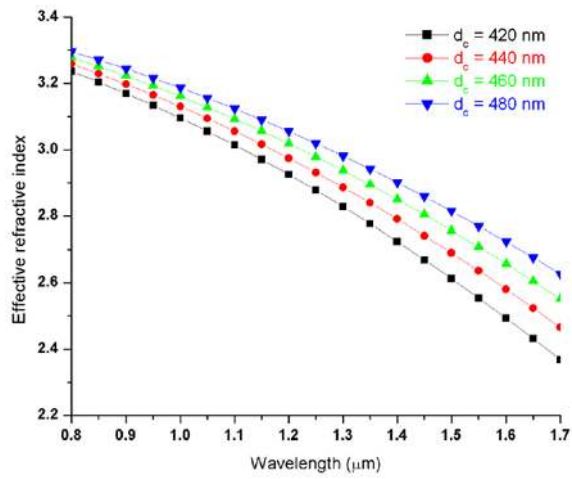

Figure 3: *Variations of effective refractive index for various core diameters of SN-PCF*
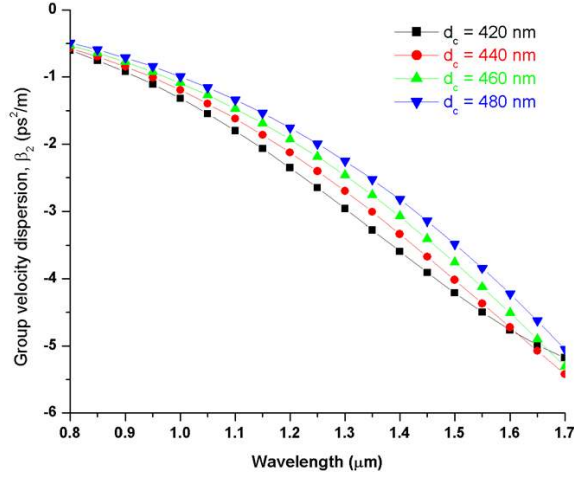
Figure 4: *Variations of group velocity dispersion of the proposed SN-PCF for different core diameters*

3.1 Waveguide dispersion

The group velocity dispersion (GVD) and third order dispersion (TOD) of the mode are determined, respectively, from the second and third derivative of the n_{eff} as a function of wavelength. We use the following equations for determining the GVD and TOD,

$$\beta_2 = \frac{\lambda^3}{2\pi c^2} \frac{d^2 n_{eff}}{d\lambda^2} \tag{1}$$

and

$$\beta_3 = -\frac{\lambda^4}{4\pi^2 c^3} \left[\lambda \frac{d^3 n_{eff}}{d\lambda^3} - 3 \frac{d^2 n_{eff}}{d\lambda^2} \right], \tag{2}$$

where λ is the wavelength, n_{eff} is the refractive index of the fundamental mode and c is the velocity of light in vacuum. In this work, we ignore the effect of material dispersion on account of the fact that its magnitude is very much lesser than that due to waveguide dispersion.

The variations of GVD and TOD with respect to wavelength for various core diameters are as shown in Fig. 4 and Fig. 5. As is seen in Fig. 4, when the core diameter is reduced from 480 nm to 440 nm, the GVD decreases upon increasing the wavelength due to the increase in field distribution towards the core-cladding boundary. However, at 420 nm core diameter, the GVD decreases up to 1.65 μm wavelength beyond which, this dispersion switches to normal regime. From the Fig. 4 it is clear that the 480 nm core diameter exhibits a less anomalous GVD (-0.4909 ps^2/m) at 0.8 μm wavelength. Further, we report a less TOD (0.6595$\times$10^{-3} ps^3/m) at 0.8 μm wavelength for 480 nm core diameter and this is evident from Fig. 5.

3.2 Effective nonlinearity

Due to the small core diameter and high nonlinear index coefficient of silicon (4$\times$10^{-18}m^2/W), the SN-PCF exhibits tight mode confinement compared to conventional PCF. But a significant fraction of the optical mode propagates in air as the evanescent field. Hence, an accurate estimation of the nonlinear coefficient γ^V is needed for small core diameter. This is carried out based on vectorially-based nonlinear Schrödinger equation (VNSE) (28):

$$\gamma^V = k_0 \left(\frac{\epsilon_0}{\mu_0} \right) \frac{\int n_0^2(x,y) n_2(x,y) |e_m|^4 dA}{|\int (e_m \times h_m^*).\hat{z} dA|^2} \tag{3}$$
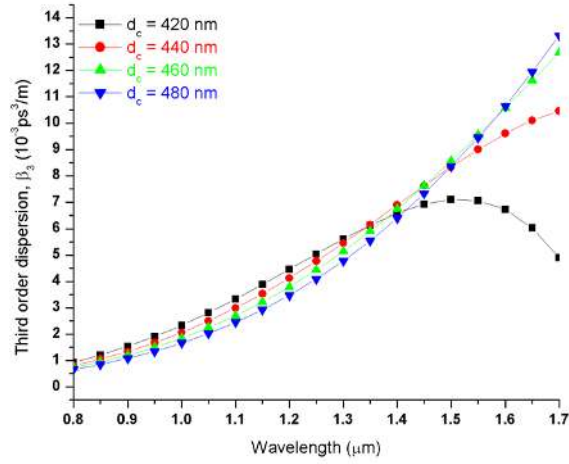
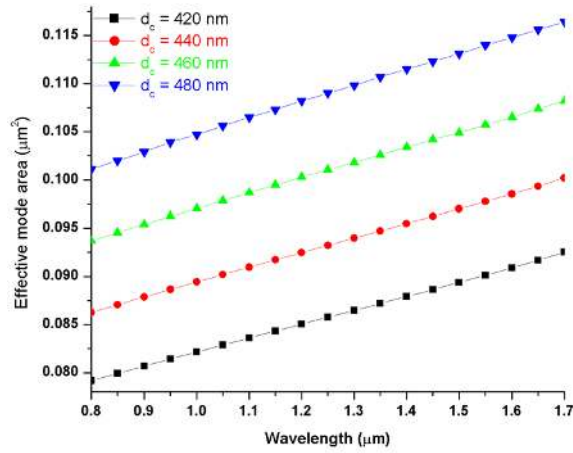**Figure 5:** *Variations of third order dispersion of the proposed SN-PCF for different core diameters*

Figure 6: *Variations of effective mode area as a function of wavelength for different core diameters*

where k_0, ϵ_0, μ_0 and n_0 are the free-space wavenumber ($2\pi/\lambda$), free-space dielectric constant, free-space permeability and refractive index of silicon, respectively. Here n_2 is the nonlinear index coefficient of silicon whose value is two orders greater than that of silica.

It is known that the mode confinement determined by the effective mode area becomes much pronounced upon reducing the core diameter of the proposed fiber. Fig. 6 depicts the variation of effective mode area with respect to wavelength for various core diameters. The results show a slowly increasing mode area with the increase in wavelength. The proposed structure possesses a minimum effective mode area for lower wavelengths at 420 nm core diameter.

Next, we proceed to compute the effective nonlinearity by using Eq. (3). Fig. 7 describes the variation of effective nonlinearity as a function of wavelength for various core diameters. As it is evident from Fig. 7, the effective nonlinearity decreases as the wavelength increases. This is due to the fact that the mode area becomes larger at higher wavelengths. For lower wavelengths, the small core diameters exhibit strong nonlinearity due to the tight mode confinement.
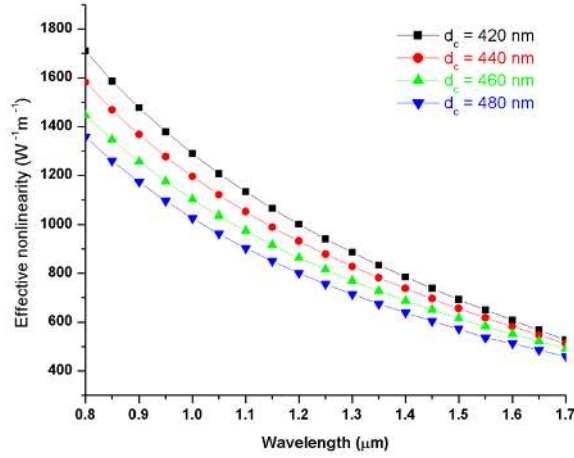
Figure 7: *Variations of effective nonlinearity for different core diameters of the proposed SN-PCFs*

4 Simulation of supercontinuum generation

The SC generation in the SN-PCF is demonstrated by the generalized higher order nonlinear Schrödinger equation (NLS) with the effects of two-photon absorbtion and free-carrier absorbtion as follows (21).

$$\frac{\partial A}{\partial z} = -\frac{1}{2}(\alpha + \alpha^f)A - \frac{i}{2}\beta_2\frac{\partial^2 A}{\partial T^2} + \frac{\beta_3}{6}\frac{\partial^3 A}{\partial T^3} + i\gamma^V\left[1 + \frac{\omega}{\omega_0}\right]A\int_{-\infty}^{\infty}\left[R(T-\tau)|A|^2\right]d\tau \qquad (4)$$

Here, A(z, T), α, α^f, β_2, β_3, γ^V and R(T-τ) represent the field envelope, linear loss, free-carrier contribution, GVD, TOD, effective nonlinearity and Raman response function, respectively. In this simulation, we ignore the effects of free carrier absorption, two photon absorption and loss owing to their insignificant role in the interaction. The nonlinear response function $R(t)$ is defined by (21),

$$R(t) = (1 - f_R)\delta(t) + f_R h_R(t). \qquad (5)$$

The above expression includes both instantaneous electronic and delayed Raman contributions, with f_R = 0.043 representing the Raman contribution to the nonlinear response. The delayed Raman response $h_R(t)$ of silicon is expressed as:

$$h_R(t) = \Omega_R^2 \tau_1 exp\left(\frac{-T}{\tau_2}\right)sin\left(\frac{T}{\tau_1}\right), \qquad (6)$$

where the parameters τ_1 (= 10 fs) and τ_2 (= 3 ps) correspond to the Raman shift and the bandwidth of the Raman gain spectrum, respectively and Ω_R is related to τ_1.

The pulse propagation in SN-PCF is studied by solving the hitherto mentioned NLS type equation using symmetrized split-step Fourier method (29). We analyze the pulse evolution of SC by considering the hyperbolic secant profile as the input pulse and the same is given by (30):

$$A(0,t) = N\sqrt{P_0}sech\left[\frac{t}{T_0}\right], \qquad (7)$$

where P_0 is the peak power of the input pulse and T_0 is the input soliton duration defined as $T_{FWHM}/1.763$. T_{FWHM} is the input pulse duration at full width at half maximum (FWHM). The soliton order, N is defined as,

$$N^2 = \frac{L_D}{L_{NL}} = \frac{\gamma P_0 T_0^2}{|\beta_2|}, \qquad (8)$$

7

Table 1: *Optical parameters of SN-PCF at 0.8 μm, 1.3 μm and 1.55 μm wavelengths for 480 nm core diameter*

Parameters	$\lambda_c = 0.8$ μm	$\lambda_c = 1.3$ μm	$\lambda_c = 1.55$ μm
$\beta_2(ps^2/m)$	-0.4909	-2.2499	-3.8404
$\beta_3(10^{-3}ps^3/m)$	0.6595	4.7787	9.4495
$\gamma\ (W^{-1}m^{-1})$	1358	714	536
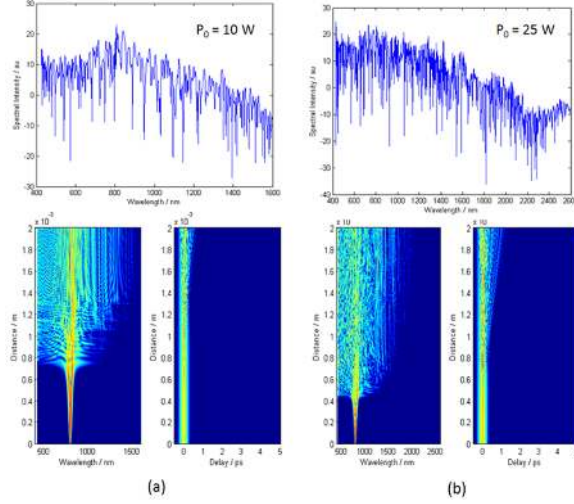
Figure 8: *Spectral, temporal evolution and intensity spectrum of the proposed SN-PCF at 0.8 μm wavelength of incident peak powers of (a) 10 W and (b) 25 W*

where L_D (= $\frac{T_0^2}{|\beta_2|}$) and L_{NL} (= $\frac{1}{T_0^2}$) are the dispersion length and nonlinear length, respectively.

We consider the propagation of a secant hyperbolic input pulse of peak power 25 W with 100 fs pulse width through the SN-PCF. We point out that, in the simulation, we consider the maximum value of core diameter (480 nm) since the proposed SN-PCF meets the requirements (less GVD with small TOD and high nonlinearity) of SC generation at 0.8, 1.3 and 1.55 μm wavelengths as tabulated in Table 1.

Figs. 8, 9 and 10 illustrate the intensity spectra of the proposed SN-PCF for various input peak powers at center wavelengths of 0.8, 1.3 and 1.55 μm, respectively. In this case, we consider the SN-PCF of length, 2 mm. From these figures, it is seen that the intensity spectra gradually get broadened and flattened upon increasing the input power, P_0 due to soliton fission and larger contribution of nonlinear effects such as self-phase modulation and Raman effect. Therefore, it is clearly seen that the SC spectral width depends on the incident power of the pulse. Figs. 11, 12, and 13 represent the intensity spectra for various lengths of the proposed SN-PCFs at the center wavelengths of 0.8, 1.3 and 1.55 μm, respectively with a peak power of 25 W. From these figures, we find that the same behaviour is noticed with the variation in length of the fiber. Hence, SC spectral width is dependent on the fiber length also.

The spectral evolution and intensity spectra of the proposed SN-PCF for 480 nm core diameter with the input peak power of 25 W with 100 fs pulse width at the wavelengths of 0.8 μm, 1.3 μm and 1.55 μm, respectively are as shown in Figs. 14, 15 and 16. The calculated SC bandwidths are 1250 nm, 1100 nm and 800 nm at the center wavelengths of 0.8 μm, 1.3 μm and 1.55 μm, respectively. From these results, it is evident that high quality SC spectrum is readily generated with relatively a short piece of fiber and a less input power due to the soliton fission and Raman effect. One of the important parameters in estimating the axial resolution of the OCT source is
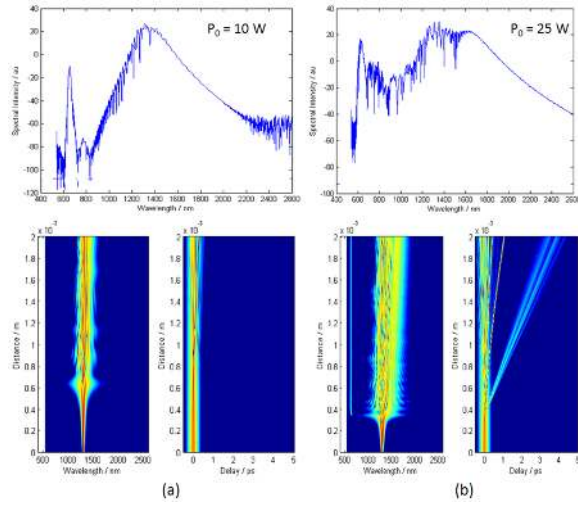
8

Figure 9: *Spectral, temporal evolution and intensity spectrum of the proposed SN-PCF at 1.3 µm wavelength of incident peak powers of (a) 10 W and (b) 25 W*

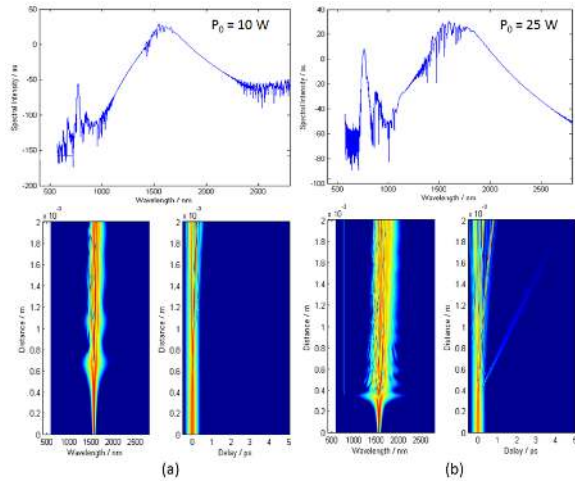**Figure 10:** *Spectral, temporal evolution and intensity spectrum of the proposed SN-PCF at 1.55 µm wavelength of incident peak powers of (a) 10 W and (b) 25 W*
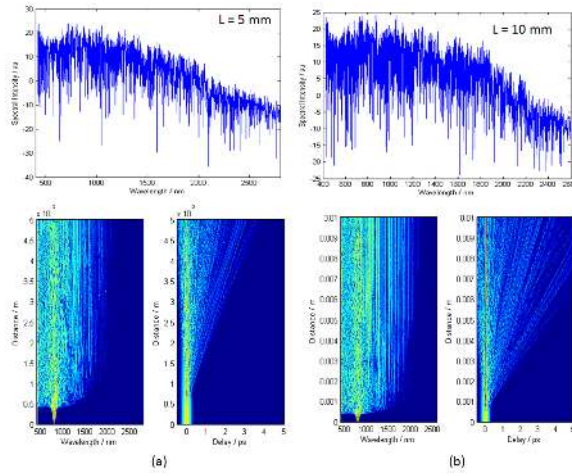
Figure 11: *Spectral, temporal evolution and spectral intensity at 0.8 µm wavelength of two different lengths of SN-PCFs (a) 5 mm and (b) 10 mm*
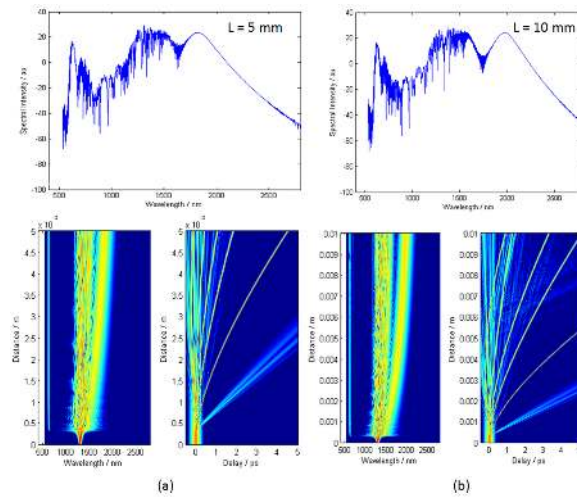

Figure 12: *Spectral, temporal evolution and spectral intensity at 1.3 µm wavelength of two different lengths of SN-PCFs (a) 5 mm and (b) 10 mm*
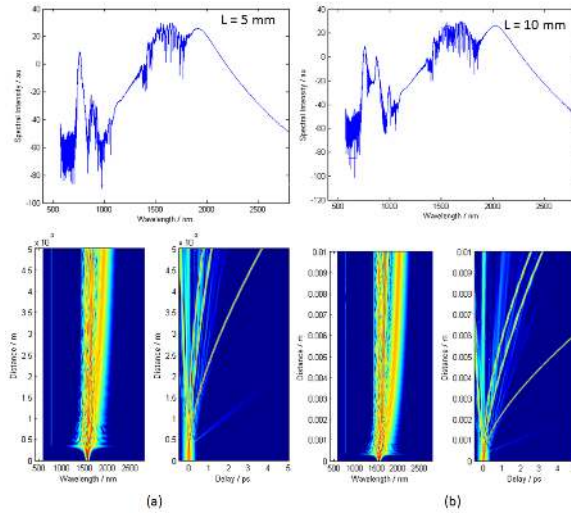
Figure 13: *Spectral, temporal evolution and spectral intensity at 1.55 μm wavelength of two different lengths of SN-PCFs (a) 5 mm and (b) 10 mm*
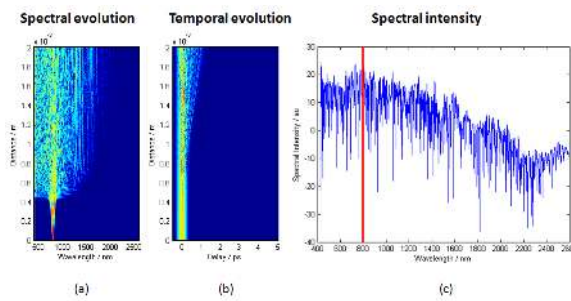

Figure 14: *(a) Spectral evolution (b) temporal evolution and (c) intensity spectrum of SC at 0.8 μm wavelength of the proposed SN-PCF using 25 W input power*

Figure 15: *(a) Spectral evolution (b) temporal evolution and (c) intensity spectrum of SC at 1.3 μm wavelength of the proposed SN-PCF using 25 W input power*

Figure 16: *(a) Spectral evolution (b) temporal evolution and (c) intensity spectrum of SC at 1.55 μm wavelength of the proposed SN-PCF using 25 W input power*
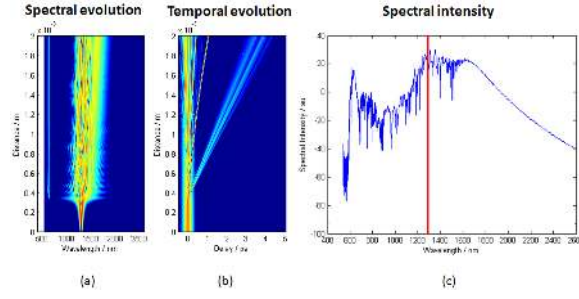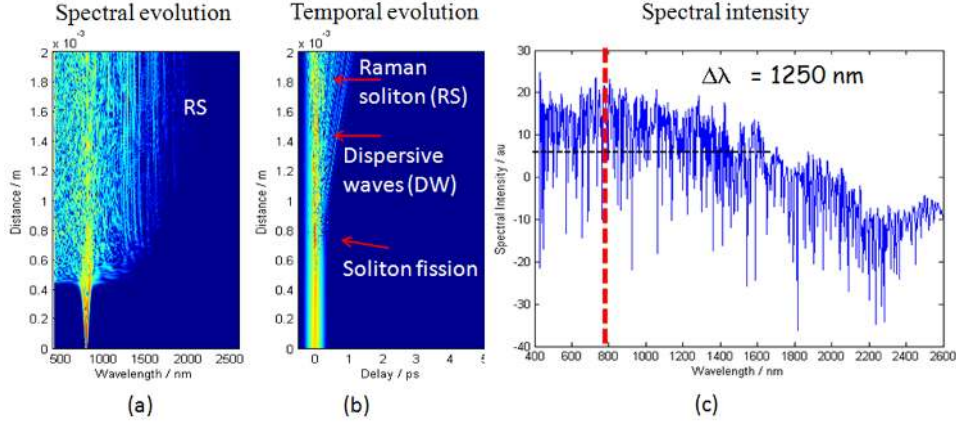
coherence length, l_c, which is given as, (4):

$$l_c = \frac{2ln2}{\pi} \frac{\lambda_c^2}{\Delta\lambda}. \tag{9}$$

Further, the axial resolution, l_r, is related to coherence length, l_c as,

$$l_r = \frac{l_c}{n_{tissue}}. \tag{10}$$

Here, n_{tissue} is the refractive index of the biomedical tissues. The calculated l_c and l_r values at 0.8 μm, 1.3 μm and 1.55 μm wavelengths are tabulated in Table 2. The calculated l_r values are 0.16 μm, 0.41 μm and 0.8 μm when typical n_{tissue} values are 1.44, 1.65 and 1.65, respectively, their corresponding centre wavelength being 0.8, 1.3 and 1.55 μm, respectively (6). These calculated l_r values are better than that of (4) as well as SLDs with OCT imaging axial resolution of approximately 10-15 μm. From Table 2, it is seen that the wider bandwidth and greater longitudinal resolution are obtained at 0.8 μm due to the small second and third order dispersions and high nonlinearity.

The proposed SN-PCF fiber can be used as a nanofiber-based light source to generate SC in three different central wavelengths for ophthalmology, dermatology and dentistry OCT imaging applications.

12

Table 2: *Calculated OCT related parameters of the 2 mm length of SN-PCF for 25 W incident peak power*

Parameters	$\lambda_c = 0.8~\mu$m	$\lambda_c = 1.3~\mu$m	$\lambda_c = 1.55~\mu$m
$\Delta\lambda$ (nm)	1250	1100	800
l_c (μm)	0.23	0.68	1.33
l_r (μm)	0.16	0.41	0.8

5   Conclusion

The proposed SN-PCF exhibits a high nonlinearity, a less small group velocity dispersion and a less third order dispersion which form the desirable requirements for realizing a broadband supercontinuum source. By solving higher order NLS type equation using split-step Fourier method, we have observed a broad bandwidth of 1250 nm at 0.8 μm wavelength when the peak power is 25 W in a short piece of SN-PCF of 2 mm. This broad bandwidth of the light source permits high resolution for bright OCT imaging in the wavelength ranges from 0.8 to 1.6 μm. The longitudinal resolutions have been computed to be 0.16 μm, 0.41 μm and 0.8 μm at center wavelengths of 0.8 μm, 1.3 μm and 1.55 μm, respectively. Thus, we envisage that the proposed SN-PCF capable of generating wider bandwidth supercontinuum might turn out to be an appropriate candidate for being deployed as a ultrahigh-resolution OCT system in various fields of medicine such as ophthalmology, dermatology, dental imaging, etc.

Acknowledgements

References

[1] H. Kopka and P. W. Daly, *A Guide to LATEX*, 3rd ed. Harlow, England: Addison-Wesley, 1999.

[2] B. Bouna, G. J. Tearney, S. A. Boppart, M. R. Hee, M. E. Brezinski, and J. G. Fujimoto, "High-resolution optical coherence tomographic imaging using a mode-locked Ti-Al$_2$O$_3$ laser source," *Opt. Lett.*, vol. 20, no. 13, pp. 1486–1488, 1995.

[3] W. Drexler, U. Morgner, F. X. Kartner, C. Pitris, S. A. Boppart, X. D. Li, E. P. Ippen, J. G. Fujimoto, "In vivo ultrahigh-resolution optical coherence tomography," *Opt. Lett.*, vol. 24, no. 17, pp. 1221–1223, 1999.

[4] Y. Namihira, M. A. Hossain, T. Koga, M. A. Islam, S. M. A. Razzak, S. F. Kaijage, Y. Hirako, H. Higa, "Design of highly nonlinear dispersion flattened hexagonal photonic crystal fibers for dental optical coherence tomography applications," *Opt. Rev.*, vol. 19, no. 2, pp. 78–81, 2012.

[5] A. Stephen Boppart, "Optical coherence tomography: Technology and applications for neuroimaging, Psychophysiology," *Blackwell Publishing Inc. Printed in the USA.*, vol. 40, no. 4, pp. 529–541, 2003.

[6] M. Ohmi, R. Yamazaki, N. Kunizawa, M. Takahashi, M. Haruna, "In vivo observation of micro-tissue structures by high-resolution optical coherence tomography with a femtosecond laser," *Japanese Society for Medical and Biological Engineering*, vol. 42, no. 4, pp. 204–210, 2004.

[7] P. R. Herz, Y. Chen, A. D. Aguirre, J. G. Fujimoto, H. Mashimo, J. Schmitt, A. Koski, J. Goodnow, C. Peterson, "Ultrahigh Resolution Optical Biopsy with Endoscopic Optical Coherence Tomography," *Opt. Exp.*, vol. 12, no. 15, pp. 3532–3542, 2004.

[8] J. H. Lee, E. J. Jung, C. S. Kim, "Incoherent, CW supercontinuum source based on erbium fiber ASE for optical coherence tomography imaging," *Proceedings of Optoelectronics and Communication Conference FD3*, pp. 13–17, 2009.

[9] Z. M. Zhu, T. G. Brown, "Experimental studies of polarization properties of supercontinua generated in a birefringent photonic crystal fiber," *Opt. Exp.*, vol. 12, no. 5, pp. 791–796, 2004.

[10] N. Haverkamp, H. R. Telle, "Complex intensity modulation transfer function for supercontinuum generation in microstructure fibers," *Opt. Exp.*, vol. 12, no. 4, pp. 582–587, 2004.

[11] Z. M. Zhu, T. G. Brown, "Polarization properties of supercontinuum spectra generated in birefringent photonic crystal fibers," *Opt. Soc. Am. B*, vol. 21, no. 2, pp. 249-257, 2004.

[12] W. J. Wadsworth, N. Joly, J. C. Knight, T. A. Birks, F. Biancalana, P. St. J. Russell, "Supercontinuum and four-wave mixing with Q-switched pulses in endlessly single-mode photonic crystal fibres," *Opt. Exp.*, vol. 12, no. 2, pp. 299–309, 2004.

[13] T. J. Hori, J. Takayanagi, N. Nishizawa, T. Goto, "Flatly broadened, wideband and low noise supercontinuum generation in highly nonlinear hybrid fiber," *Opt. Exp.*, vol. 12, no. 2, pp. 317–324, 2004.

[14] A. V. Husakou, J. Herrmann, "Supercontinuum generation in photonic crystal fiber made from highly nonlinear glasses," *Appl. Phys. B*, vol. 77, no. 2-3, pp. 227–234, 2003.

[15] G. E. Town, T. Funaba, T. Ryan, K. Lyytikainen, "Optical supercontinuum generation from nanosecond pump pulses in an irregularly microstructured air-silica optical fiber," *Appl. Phys. B*, vol. 77, no. 2-3, pp. 235–238, 2003.

[16] K. M. Hilligsoe, H. N. Paulsen, J. Thogersen, S. R. Keiding, J. J. Larsen, "Initial steps of supercontinuum generation in photonic crystal fibers," *J. Opt. Soc. Am. B*, vol. 20, no. 9, pp. 1887-1893, 2003.

[17] K. Saitoh, M. Koshiba, "Highly nonlinear dispersion-flattened photonic crystal fibers for supercontinuum generation in a telecommunication window," *Opt. Exp.*, vol. 12, no. 10, pp. 2027–2032, 2004.

[18] A. V. Husakou, J. Herrmann, "Supercontinuum Generation of Higher-Order Solitons by Fission in Photonic Crystal Fibers," *Phys. Rev. Lett.*, vol. 87, no. 20, pp. 203901–203904, 2001.

[19] M. Foster, A. L. Gaeta, Q. Cao, R. Trebino, "Soliton-effect compression of supercontinuum to few-cycle durations in photonic nanowires," *Opt. Exp.*, vol. 13, no. 18, pp. 6848–6855, 2005.

[20] O. Boyraz, P. Koonath, V. Raghunathan, B. Jalali, "All optical switching and continuum generation in silicon waveguides," *Opt. Exp.*, vol. 12, no. 17, pp. 4094–4102, 2004.

[21] L. Yin, Q. Lin, G. P. Agrawal, "Soliton fission and supercontinuum generation in silicon waveguides," *Opt. Lett.*, vol. 32, no. 4, pp. 391–393, 2007.

[22] J. B. Driscoll, X. Liu, S. Yasseri, I. Hsieh, J. I. Dadap, R. M. Jr. Osgood, "Large longitudinal electric fields (E_z) in silicon nanowire waveguides," *Opt. Exp.*, vol. 17, no. 4, pp. 2797–2804, 2009.

[23] F. Biancalana, V. Tran, S. Stark, M. A. Schmidt, P. St. J. Russell, "Emergence of geometrical optical nonlinearities in photonic crystal fiber nanowires," *Phys. Rev. Lett.*, vol. 105, no. 9, pp. 093904–093907, 2010.

[24] E. Gunasundari, K. Senthilnathan, S. Sivabalan, M. Abdosllam Abobaker, K. Nakkeeran, P. Ramesh Babu, "Waveguiding properties of a silicon nanowire embedded photonic crystal fiber," *Opt. Mater.*, vol. 36, no. 5, pp. 958–964, 2014.

[25] L. Tong, J. Lou, E. Mazur, "Single-mode guiding properties of subwavelength-diameter silica and silicon wire waveguides," *Opt. Exp.*, vol. 12, no. 6, pp. 1025–1035, 2004.

[26] A. B. Salem, R. Cherif, M. Zghal, "Low-energy single-optical-cycle soliton self-compression in air-silica nanowires," *J. Nanophoton.*, vol. 5, no. 1, pp. 059506(1-6), 2011.

[27] A. B. Salem, R. Cherif, M. Zghal, "Soliton-self compression in highly nonlinear chalcogenide photonic nanowires with ultralow pulse energy," *Opt. Exp.*, vol. 19, no. 21, pp. 19955–19966, 2011.

[28] S. V. Afshar, T. M. Monro, "A full vectorial model for pulse propagation in emerging waveguides with subwavelength structures partI: Kerr nonlinearity," *Opt. Exp.*, vol. 17, no. 4, pp. 2298–2318, 2009.

[29] J. M. Dudley, J. R. Taylor, Supercontinuum Generation in Optical Fibers, Cambride University Press, 2010.

[30] G. P. Agrawal, Nonlinear Fiber Optics, Academic Press, 2007.